Energy & Environmental Science

COMMUNICATION

Efficient planar heterojunction mixed-halide perovskite solar cells deposited *via* spray-deposition†

Alexander T. Barrows,[a] Andrew J. Pearson,‡[a] Chan Kyu Kwak,[b] Alan D. F. Dunbar,[b] Alastair R. Buckley[a] and David G. Lidzey*[a]

Cite this: *Energy Environ. Sci.*, 2014, **7**, 2944

Received 19th May 2014
Accepted 9th July 2014

DOI: 10.1039/c4ee01546k

www.rsc.org/ees

We report the use of ultra-sonic spray-coating under ambient conditions as a deposition technique for the fabrication of planar heterojunction $CH_3NH_3PbI_{3-x}Cl_x$ perovskite solar cells. We make a first optimization of processing parameter space using this deposition technique, and explore the role of the temperature of the substrate during spray-casting, the volatility of the casting solvent and the post deposition anneal on determining the efficiency of the resultant solar cells. We find that maximum device efficiency is correlated with the creation of dense films having a surface coverage above 85%. When such films are incorporated into a solar cell device, power conversion efficiencies of up to 11% are realized. These results demonstrate that spray-coating can be used in the large-area, low-cost manufacture of high efficiency solution-processed perovskite solar cells.

Broader context

Sunlight offers vast potential to decarbonise the world economy *via* the widespread implementation of solar energy harvesting technologies. Photovolatic devices significantly contribute to this area, however a present drawback to their extensive adoption is the cost associated with manufacturing efficient modules. Solution processable organic–inorganic perovskite semiconductors have recently emerged as promising light-harvesting materials in photovoltaic devices. Remarkably, this class of material offers the potential to combine the high-performance of existing technologies with the low embedded cost of production traditionally associated with thin-film organic PV. Driven by these exciting characteristics, perovskite PV is currently attracting significant interest within the photovoltaic research community in order to determine the commercially viable processing protocols for manufacture. Here, we successfully demonstrate the fabrication of perovskite solar cells with an efficiency of up to 11%, where the light-harvesting layer has been deposited by spray-coating. This study advances upon existing work where the perovskite layer has been deposited from solution using laboratory scale techniques such as spin-coating, and represents a significant step in the development of efficient, low-cost solar cell devices made using roll-to-roll compatible processing methods.

Introduction

The rapid rise in efficiency of thin-film solar cells using organometal halide perovskite semiconductors has made this class of photovoltaic device a highly promising technology for solar energy conversion.[1–3] State-of-the-art devices already achieve power conversion efficiencies (PCEs) of 15–16%;[4–6] this value surpassing the record efficiencies of amorphous silicon and organic semiconductor PV.[7] The precursor materials used to fabricate perovskite films can be deposited from solution,[8] enabling processing routes with low embodied energy to be used in the fabrication of functional devices. To date however, there have been few reports of scalable solution-processing techniques being applied to the deposition of perovskite films. It is apparent that the path towards commercialization of solution-processed perovskite solar cells requires the development of fabrication protocols compatible with high-volume roll-to-roll or sheet-fed processing techniques. Such techniques should ideally result in the creation of devices having power conversion efficiencies similar to those already demonstrated using non-scalable deposition processes such as spin-casting. We note that the development of scalable deposition technologies is an active area of research within the field of polymer:fullerene bulk-heterojunction Organic Photovoltaics (OPVs).[9–11] Here, a number of scalable techniques have been evaluated for large-area device processing, including ink-jet printing,[12,13] slot-die coating[14,15] and spray-coating.[16–19] Notably, the optimized ink formulations of polymer:fullerene blends are not necessarily transferrable between each of these techniques as a result of the different mechanisms that drive film formation.[9,11] Understanding such differences is an important aspect of the development of solution-based PV deposition processes suitable for manufacture at large-scale.

[a]*Department of Physics & Astronomy, University of Sheffield, Hicks Building, Hounsfield Road, Sheffield, S3 7RH, UK. E-mail: d.g.lidzey@sheffield.ac.uk; Fax: +44 (0)114 222 3555; Tel: +44 (0)114 222 3501*

[b]*Department of Chemical and Biological Engineering, University of Sheffield, Sir Robert Hadfield Building, Mappin St., Sheffield S1 3JD, UK*

† Electronic supplementary information (ESI) available: Additional optical micrographs, XRD spectra and distribution of device efficiencies (including the effects of light-soaking). See DOI: 10.1039/c4ee01546k

‡ Present address: Cavendish Laboratory, JJ Thomson Avenue, Cambridge CB3 0HE, UK.

In this work, we explore the use of ultra-sonic spray-coating as a deposition technique to create thin-films of a perovskite precursor containing methylammonium iodide and lead chloride in ambient conditions.[8] These films are subsequently annealed into a $CH_3NH_3PbI_{3-x}Cl_x$ perovskite structure, and fabricated into a solar cell device having a planar heterojunction architecture.[20–22] We identify an important parameter space associated with the temperature of the substrate during precursor deposition and subsequent annealing that influences the surface coverage of the perovskite over the underlying substrate.[20,23,24] We note that previous reports of spin-coated planar heterojunction solar cells using $CH_3NH_3PbI_{3-x}Cl_x$ deposited from a single precursor solution have achieved average PCEs in the range 6–8% (ref. 4, 20, 21 and 25) with a range of hole- and electron-transporting semiconductors, with champion devices exhibiting PCEs of up to 11%;[21,22,25] a result that we replicate here. Such figures-of-merit compare favourably with solar cells made using single halide semiconductors, incorporated in either a planar or mesoporous scaffold architecture[5,25–29] in which sequential processing of the perovskite film affords the possibility of PCEs of up to 15%.[5,29] We believe however that significant scope exists to further improve the efficiency and yield of spray-cast devices; a process that will be dependent upon the quality of the deposited perovskite films over large areas. Indeed, we find that high efficiency devices are correlated with optically thick and continuous perovskite layers that are free from pinholes and areas void of perovskite.[4,30] Such voids in a perovskite film will provide paths of low shunt resistance between the electrodes of the solar cell that will act to reduce the maximum attainable open-circuit voltage V_{OC} and fill factor FF.

For the samples prepared in this work a range of optical and structural probes are used to characterize the effects of different spray-coating conditions on film quality. Our optimized low-temperature (<100 °C) processing protocol results in the fabrication of solar cells with an average efficiency of 7.8%. Our best device exhibits a PCE of 11.1%, a value comparable to other champion devices based on spin-cast $CH_3NH_3PbI_{3-x}Cl_x$ films utilising PEDOT:PSS and PCBM electrode interfacial layers,[21,22] and is the highest efficiency reported for spray-deposited PV to date. These results demonstrate the promise of spray-coating as a scalable technique for the large-area deposition of perovskite films for solar cell applications.

Results and discussion

The spray-coating system used in this work has previously been used in the deposition of uniform metal oxide and polymer:fullerene blend thin-films for OPV applications.[18,31] One of the key characteristics of the system is the nozzle-less spray head that permits the generation of an ultra-fine aerosol upon contact of the spray solution with an ultra-sonic (35 kHz) vibrating tip. Here, the advantage over nozzle-based spray-deposition is the minimization of droplet coalescence before reaching the substrate, as the coalescence of droplets within a nozzle results in larger droplets that negatively impact upon film uniformity.[32,33] This approach provides a means for efficient thin-film deposition with minimal material wastage, allowing films to be cast from inks containing a lower solid concentration compared to techniques such as spin-coating.

We have deposited perovskite precursor films of methylammonium iodide (MAI) and $PbCl_2$ in a single pass of the spray-head over the solar cell substrate. After conversion *via* thermal annealing to $CH_3NH_3PbI_{3-x}Cl_x$, these films were incorporated into planar-heterojunction solar cells within the device architecture ITO/PEDOT:PSS/perovskite/PCBM/Ca/Al, with PEDOT:PSS and PCBM/Ca acting as hole- and electron-transporting layers respectively. We note that the boiling point (b.p.) of the casting solvent is an important factor in influencing the quality of the spray-deposited films. Previous work on spray-coating polymeric organic semiconductors from a chloroform solvent[18] (b.p. 63 °C) has shown that if the boiling point is too low, the spray solution can dry before reaching the substrate resulting in a film characterized by a relatively large density of pinholes and significant thickness variations, making such films unsuitable for PV applications. Here, the boiling points of the casting solvents are relatively high, having values of 153 °C and 189 °C for dimethylformamide (DMF) and dimethylsulfoxide (DMSO) respectively. Such relatively high boiling points can result in the formation of large-area thickness variations or shrinkage/de-wetting of the casting solution due to the relatively prolonged drying times of spray-coated films. To minimize such issues we have designed a process by which the casting solution is sprayed onto a substrate held at an elevated temperature to accelerate the film drying process. This is then followed by a second, extended thermal anneal to crystallize the MAI:$PbCl_2$ precursor film into a $CH_3NH_3PbI_{3-x}Cl_x$ perovskite structure. This extended thermal anneal also removes excess solvent and organic and halide materials.[20]

In Fig. 1 we present a series of optical micrographs that show the effect of the substrate temperature during deposition on the quality of the as-deposited films. Here, each film was spray-cast from a perovskite precursor dissolved in DMF and then subject to a post-film deposition thermal anneal at 90 °C for 90 minutes. The nominal thickness of each film is in the range of 230 to 270 nm, as measured by profilometry. It can be seen that relatively low substrate temperatures during solution deposition (corresponding to relatively prolonged drying times) are correlated with perovskite films having a low substrate coverage. Indeed, it is apparent in Fig. 1 parts (a) and (b) that there are relatively large and discontinuous crystalline regions on the film substrate; with films deposited onto a substrate held at 28 °C having an average substrate coverage as low as (65 ± 5)%. As the substrate temperature during spray-deposition is increased, we find that the perovskite films become more continuous and are characterized by a hierarchy of structures on a micron length-scale. Indeed, we find that the surface coverage of perovskites on a PEDOT:PSS/ITO substrate takes a maximum value of (85 ± 5)% when the precursor film is deposited onto a substrate held at 75 °C (see Fig. 1 part (d)).

To optimize the post-deposition annealing treatment, we spray-cast a series of precursor-perovskite onto substrates heated to 75 °C, that were then annealed at temperatures ranging between 70 and 130 °C for times ranging between

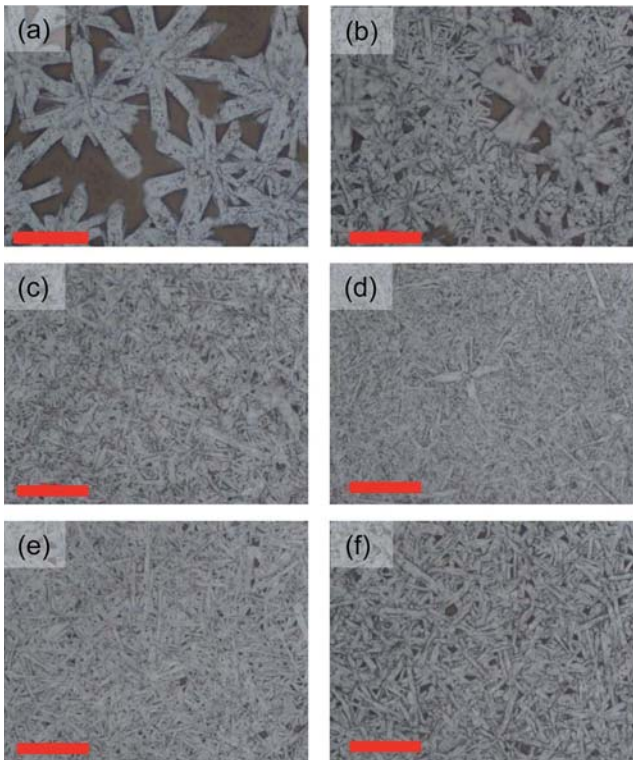

Fig. 1 Optical microscopy images of spray-deposited thin-films of methylammonium iodide and lead chloride onto substrates held at a range of elevated temperatures. (a) 28 °C, (b) 38 °C, (c) 55 °C, (d) 75 °C, (e) 80 °C, (f) 87 °C. The scale bar in each image corresponds to 20 μm.

30 and 90 minutes. Samples were characterized using optical microscopy, with data shown in ESI Fig. S1.† For samples annealed at a temperature ≤90 °C for 30 minutes, the perovskite films have color variations across their surface suggesting incomplete crystallization. These results are in qualitative agreement with detailed studies on the thermal annealing protocol of MAI and $PbCl_2$,[24] where it was found that low annealing temperatures required extended annealing-times above 3 hours to fully crystallize the perovskite film. At annealing temperatures above 110 °C, we find that the film perovskite film undergoes partial dewetting, leading to a relatively low surface coverage. At the highest annealing temperature trialed in this study (130 °C), the films formed again have significant variations in color, with a number of regions characterized by a yellow hue. This observation suggests that the perovskite layer has partially decomposed into regions rich in PbI_2.[24]

To understand the role played by the casting solvent on controlling the surface coverage of a perovskite film, a set of films were prepared by spray-casting the precursor solution from DMSO. Optical micrographs of films cast using the same conditions as in Fig. 1 are presented in ESI Fig. S2.† Here, we find that such films have a relative reduction in perovskite surface coverage compared to films cast from DMF. Films cast on to substrates held at or below 38 °C also undergo significant de-wetting owing to the prolonged (c. 20 minutes) drying time. At temperatures between 55 °C and 80 °C, we observe the formation of relatively large perovskite crystals, however the surface coverage does not exceed (65 ± 5)%. These results are in qualitative agreement with earlier reports on films cast from DMSO,[20] suggesting that relatively slow film formation dynamics have a detrimental impact on the formation of continuous perovskite layers during subsequent annealing. Here, the peak PCE from solar cells prepared using DMSO solvent is 4.8% (see ESI Fig. S3†). A detailed study on the kinetics of perovskite formation is currently underway to further explore this process.

A series of photovoltaic devices were fabricated to evaluate the PCE of PSCs deposited by spray-casting from DMF. Here, precursor films were deposited at a substrate temperature of 75 °C (corresponding to a film drying time of less than 1 minute) and then annealed at 90 °C for 90 minutes; conditions that correspond to maximal surface coverage of the perovskite film. The morphology of such films were also characterized using scanning electron microscopy (SEM), X-ray Diffraction (XRD) and scanning probe microscopy (SPM), with results presented in Fig. 2. It can be seen from the SEM shown in Fig. 2(a) that the film created is characterized by a series of voids; a result in accord with the optical microscopy images shown in Fig. 1. The presence of such voids are also apparent in Fig. 2(b) where we plot an SEM image taken across the cleaved edge of a PEDOT:PSS/perovskite/PCBM/Ca/Al film deposited on a silicon wafer.

In Fig. 2(c) we plot an XRD 2θ scan recorded from a spray-cast perovskite film deposited on a PEDOT:PSS/glass substrate, and thermally annealed according to the optimised conditions discussed previously. We attribute the relatively strong diffraction signals at 14.2°, 28.6° and 43.8° to X-ray scatter from the (110), (220) and (330) planes of tetragonal $CH_3NH_3PbI_{3-x}Cl_x$ respectively.[4,8,24] Note however that additional peaks are resolvable in

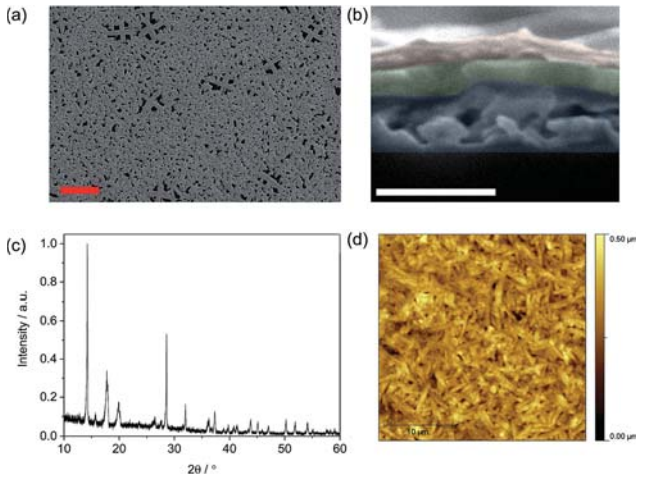

Fig. 2 (a) SEM image of spray-deposited $CH_3NH_3PbI_{3-x}Cl_x$ on PEDOT:PSS. Here the scale bar corresponds to 50 μm. (b) Cross-sectional SEM image of the solar cell architecture PEDOT:PSS/$CH_3NH_3PbI_{3-x}Cl_x$/PCBM/Ca/Al employed in this work. The perovskite, PCBM and Ca/Al layers are highlighted in blue, green and orange respectively to ease identification. Here the scale bar corresponds to 1 μm. (c) XRD pattern of spray-deposited $CH_3NH_3PbI_{3-x}Cl_x$ on PEDOT:PSS. (d) SPM image of the surface topography of the perovskite thin-film.

the diffraction spectrum. These peaks are also present in measurements of nominally identical perovskite films deposited onto silicon (see ESI Fig. S4†) and may correspond to $PbCl_2$ as has been observed elsewhere.[24] This observation is consistent with an incomplete conversion of precursor material into $CH_3NH_3PbI_{3-x}Cl_x$. Nevertheless, as will be demonstrated below, PV devices based on such films still have very promising efficiency. In Fig. 2(d), we plot the topography of the perovskite film characterized by SPM. The film has an RMS roughness of 50 nm, however this value masks significant local height variations in areas void of perovskite, with such variations being commensurate with the film thickness (c. 270 nm as measured by profilometry).

A series of PV devices were fabricated using the optimized perovskite/PEDOT:PSS layer together with a PCBM electron-extraction layer. Here, a relatively thick PCBM layer was used (having a thickness of around 120 nm) to minimize short-circuits between the solar cell electrodes at places corresponding to voids in the perovskite film (see Fig. 2(b)). Our optimization process also included a study of perovskite layer thickness, with films explored having a thickness ranging between 300 and 700 nm. The average solar cell efficiency metrics of solar cell devices fabricated and the results for the "champion cell" are summarized in Table 1. As shown in Table 1, devices with an active layer of thickness of 340 ± 30 nm exhibit relatively high PCE combined with narrow distribution in film thickness variations. A second, larger study was then conducted utilizing perovskite films having this thickness range (44 cells tested), with solar cells exhibiting an average PCE of 7.8 ± 2%. For the best solar cell, a PCE of 11.1% was determined. This value matches an earlier report of mixed-halide perovskite planar heterojunction solar cells utilizing PEDOT:PSS and PCBM electrode interfacial layers.[21] The current-voltage characteristics for the champion cell are presented in Fig. 3(a) with the external quantum efficiency for a typical cell plotted in Fig. 3(b). Using this data, we calculate the theoretical J_{SC} for our device, and find it to be within 5% of its measured value. For completeness, we have also fabricated a series of solar-cells using the same materials set, however using a spin-coated to deposit the perovskite precursor solution (see Experimental methods). As can be seen from Table 1 and Fig. 3(c), spin- and spray-cast devices have similar average PCE, indicating that the spray-coating process does not apparently reduce cell efficiency.

We note that during the measurement of all perovskite cells, a positive light-soaking effect on enhancing device PCE was observed during the first 20 minutes of illumination. This treatment was applied whilst the solar cells were held at open-circuit, and resulted in a simultaneous increase in device FF, J_{SC} and V_{OC} (see ESI† for further details). In planar-heterojunction

Table 1 Average solar cell metrics and standard deviations for each processing batch of perovskite solar cell under simulated 100 mW cm^{-2} AM1.5G illumination. Devices were left under the solar simulator for 20 minutes prior to measurement. To remove any selection bias, these averages represent the top 50% of pixels in each processing batch (10 individual cells during initial thickness test, 22 cells for a layer thickness of 360 nm). The champion cell metrics corresponds to the data presented in Fig. 3. * Perovskite layer deposited *via* spin-coating of the precursor solution

Perovskite layer thickness (nm)	J_{SC}/mA cm^{-2}	V_{OC}/V	FF/%	PCE/%
290 ± 30	−10.8	0.73	42	3.3 ± 2.0
340 ± 30	−15.2	0.78	55	6.5 ± 0.8
450 ± 40	−10.4	0.86	56	5.0 ± 0.5
670 ± 200	−12.2	0.87	57	6.0 ± 0.3
330 ± 40	−14.9	0.84	63	7.8 ± 2
Champion cell	−16.8	0.92	72	11.1
400 ± 10*	−13.7	0.85	67	7.8 ± 0.3

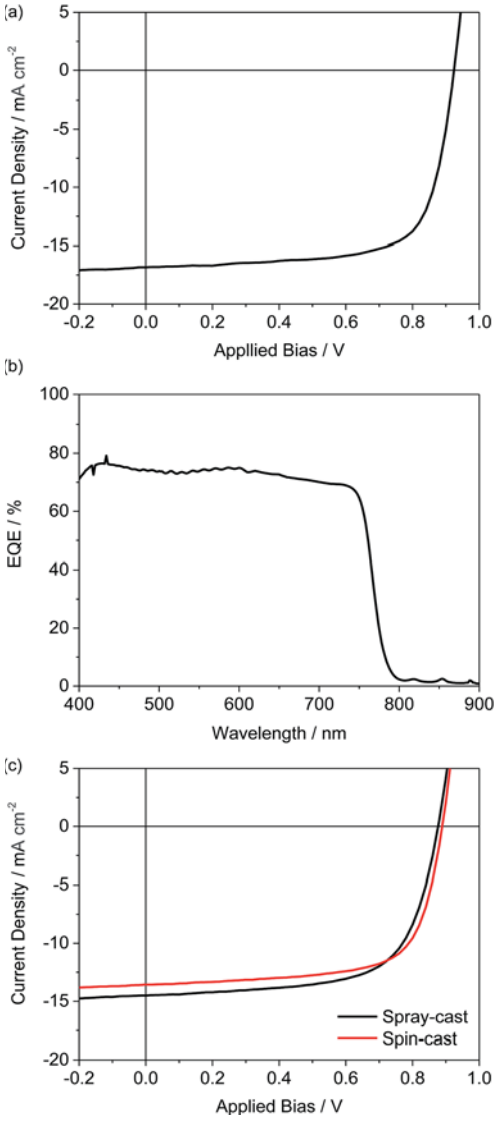

Fig. 3 (a) Current-density *versus* voltage characteristics for spray-deposited $CH_3NH_3PbI_{3-x}Cl_x$ planar solar cell subject to optimised processing conditions. (b) External quantum efficiency spectrum for the same cell, corresponding to an integrated J_{SC} of 17.7 mA cm^{-2} with respect to the AM1.5G solar spectrum. (c) Comparison of average current-density *versus* voltage characteristics for perovskite solar cells where the light-harvesting layer has been deposited *via* either spray-coating or spin-coating.

perovskite solar cells incorporating TiO_x as a cathode buffer layer, positive light-soaking effects have also been observed that were specifically attributed to the presence of TiO_x.[21] As this material is not present in our devices, this suggests that the light-soaking may be influencing a mechanistically distinct process.

A final characterization of device efficiency was conducted to determine the magnitude of the hysteresis effects in cell performance.[34] Here, a solar cell with an average PCE of 8.4% was subject to a series of current–voltage measurements where both the scan rate and scan-direction were varied (although the influence of the absolute starting bias was not explored). Our results are presented in Fig. 4. We find that under the measurement conditions investigated here, there is a marginally higher PCE is determined on measuring from forward (1 V) to reverse (−1 V) bias. Note however the difference in PCE determined between each measurement is approximately 6%; a value within the cell-to-cell variation of the processing batch.

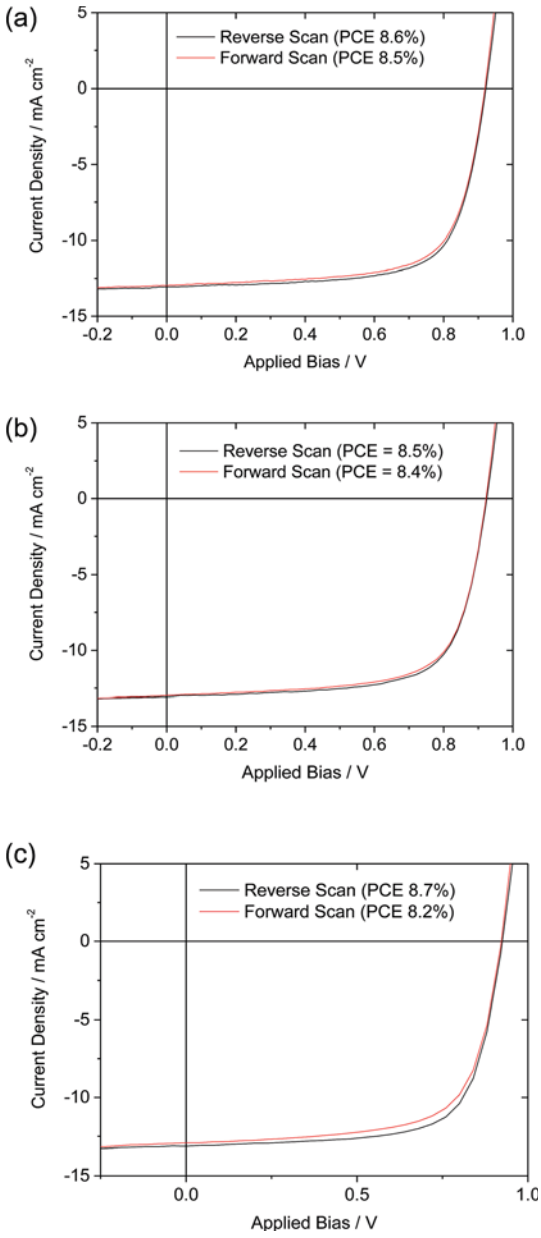

Fig. 4 Current-density *versus* voltage characteristics for a perovskite solar cell device measured under different scan rates and scan directions: (a) 0.5 V s^{-1}, (b) 1 V s^{-1} and (c) 2 V s^{-1}. Efficiency values are shown in each figure legend. Note that the forward bias sweep conditions reported in part (b) correspond to our standard testing protocol.

Conclusions

The evaluation of scalable deposition techniques for solution processable perovskite semiconductor films is a necessary process in the path towards their low-cost manufacture. To address this, we have explored the use of spray-coating under ambient conditions to deposit a blend of methylammonium iodide and lead chloride from solution, with such films subjected to a thermal annealing step to crystallize the precursor into a $CH_3NH_3PbI_{3-x}Cl_x$ perovskite film. Such films were subsequently fabricated into planar-heterojunction solar cell devices. Our optimized processing route results in solar cells having power conversion efficiencies of up to 11%, with no loss in average PCE determined compared to cells fabricated by spin-coating the perovskite precursor layer. We note that the slow (90 minute) annealing process employed here may be reduced *via* the use of techniques such as flash-annealing[35] and IR heating. Furthermore, the use of sequential steps to deposit the perovskite precursor compounds also offers an alternative route for scalable film processing that in principle removes the need for thermal annealing at elevated temperatures. Our work demonstrates therefore that spray-coating can be used as a practical technique to deposit precursor perovskite films that can then be used in high-performance photovoltaic devices with a range of electrode interfacial layers. We believe this result is an important step towards the commercialization of this technology.

Experimental

Preparation of perovskite precursor

Methylamine (33 wt% in ethanol), hydroiodic acid (57 wt% in water) and lead II chloride (98% purity) were purchased from Sigma Aldrich and were used as received. Synthesis of methylammonium iodide powder followed methods described in detail elsewhere.[4] The powder was dried overnight in a vacuum oven at 40 °C before use. Precursor solutions of methylammonium iodide and lead chloride (3 : 1 molar ratio) were dissolved in sequence into dimethylformamide (DMF) or dimethylsulfoxide (DMSO) to a total concentration of 100 mg ml^{-1}. For spin-coated films, a solution with a total solids concentration of 664 mg ml^{-1} was used. Solutions were heated at 70 °C overnight to encourage dissolution of solid material, cooled to room temperature, and then filtered through a 0.45 μm PTFE filter before use.

Perovskite solar cell device fabrication

Pre-patterned glass-ITO substrates (20 Ω $\square^{-1}$) were purchased from Ossila Limited. The substrates were cleaned by sonication

in Helmanex solution, isopropyl alcohol and deionized water and dried with compressed nitrogen before use. PEDOT:PSS (HC Stark Clevios P VP AI4083, filtered through a 0.45 μm PVDF filter) was spin cast on top of the cleaned substrates to form a 30 nm thick layer that was then annealed in air at 130 °C for 30 minutes prior to use. The precursor perovskite films were then coated on the ITO/PEDOT:PSS anode under ambient conditions using a Prism ultrasonic spray-coating system supplied by Ultrasonic Systems, Inc. (USI). This system uses a fixed ultrasonic frequency of 35 kHz and a nitrogen-gas carrier pressure of 10 psi. Films were sprayed at a nozzle height of 45 mm and lateral speed between 20 and 200 mm s^{-1}. During spray-coating, substrates were held at a fixed temperature, after which they were transferred to a second hot-plate for extended thermal annealing (with all processes performed in air). For spin-coated samples, a spin-speed of 5000 rpm was used to prepare films of the desired thickness. Prior to film deposition, both the substrate and casting solution were held at elevated temperatures (90 °C and 70 °C respectively) to enable rapid drying of uniform thin-films. For all samples, film thickness was determined from post-annealed films across 8 locations using profilometry. PCBM (99% supplied by Ossila Ltd) thin-films were deposited on to the perovskite layers by spin-coating in a glove-box. PCBM solutions for spin-coating were prepared in a 50 mg ml^{-1} chlorobenzene solution that was heated at 70 °C for 12 hours and then filtered through a 0.45 μm PTFE filter. The cathode (a bilayer of calcium and aluminium – 5 nm and 100 nm respectively) was thermally evaporated within a vacuum chamber held at a pressure $<10^{-6}$ mbar. Devices were encapsulated using a UV-treated epoxy (supplied by Ossila Ltd) before testing.

Film characterization

To estimate perovskite surface coverage, optical microscopy images were analyzed using the ImageJ software package. SPM measurements of sample surfaces were acquired using a Veeco (Santa Barbara) Dimension 3100, operating in tapping mode. Tips from Budget Sensors (300G-Al) were used, with a resonant frequency at ~300 kHz and a spring constant of ~40 N m^{-1}. Images were analysed using the Gwyddion software package. 2θ scans of X-ray diffraction from perovskite samples were obtained using a Bruker D8 X-ray Diffractometer. SEM images of samples on Si substrates were acquired using a Jeol JSM6010LA microscope.

Device characterization

Device performance was tested in ambient conditions using a Newport 92251A-1000 solar simulator (AM1.5). An NREL certified silicon reference cell was used to calibrate the integrated light-output from the simulator to 100 mW cm^{-2} at 25 °C. Here, an aperture mask (0.025 cm^2) was placed over each solar cell to accurately define the device area and minimize absorption of stray light. PCEs are determined for a cell initially held at −1 V and swept to 1 V at a rate of 1 V s^{-1} unless otherwise stated. EQE measurements of solar cell devices were acquired under continuous illumination of monochromated light from a tungsten lamp. EQE values were determined over the wavelength range of interest by comparing the photocurrent of the perovskite solar cell to a reference silicon photodiode having a known spectral response.

Acknowledgements

We acknowledge financial support from the EPSRC *via* grant EP/I028641/1 "Polymer/fullerene photovoltaic devices: new materials and innovative processes for high-volume manufacture" and from the Supergen Supersolar Hub EP/J017361/1. AB thanks the ESPRC for funding *via* the E-Futures Doctoral Training Center in Interdisciplinary Energy Research EP/G037477/1. AJP thanks King Abdulaziz University under grant no. D-004/431 for financial support. We thank Ben Stevens for assistance with the XRD measurements. We thank Lucy Pickford for assistance with the Table of Contents image.

References

1 H. J. Snaith, *J. Phys. Chem. Lett.*, 2013, **4**, 3623–3630.
2 M. D. McGehee, *Nature*, 2013, **501**, 323–325.
3 G. Hodes, *Science*, 2013, **342**, 317–318.
4 M. Z. Liu, M. B. Johnston and H. J. Snaith, *Nature*, 2013, **501**, 395–398.
5 J. Burschka, N. Pellet, S. J. Moon, R. Humphry-Baker, P. Gao, M. K. Nazeeruddin and M. Gratzel, *Nature*, 2013, **499**, 316–319.
6 D. Y. Liu and T. L. Kelly, *Nat. Photonics*, 2014, **8**, 133–138.
7 M. A. Green, K. Emery, Y. Hishikawa, W. Warta and E. D. Dunlop, *Prog. Photovoltaics*, 2014, **22**, 1–9.
8 M. M. Lee, J. Teuscher, T. Miyasaka, T. N. Murakami and H. J. Snaith, *Science*, 2012, **338**, 643–647.
9 F. C. Krebs, *Sol. Energy Mater. Sol. Cells*, 2009, **93**, 394–412.
10 F. C. Krebs, N. Espinosa, M. Hosel, R. R. Sondergaard and M. Jorgensen, *Adv. Mater.*, 2014, **26**, 29–39.
11 R. R. Sondergaard, M. Hosel and F. C. Krebs, *J. Polym. Sci., Part B: Polym. Phys.*, 2013, **51**, 16–34.
12 C. N. Hoth, P. Schilinsky, S. A. Choulis and C. J. Brabec, *Nano Lett.*, 2008, **8**, 2806–2813.
13 C. N. Hoth, S. A. Choulis, P. Schilinsky and C. J. Brabec, *Adv. Mater.*, 2007, **19**, 3973–3978.
14 B. Zimmermann, H. F. Schleiermacher, M. Niggemann and U. Wurfel, *Sol. Energy Mater. Sol. Cells*, 2011, **95**, 1587–1589.
15 F. C. Krebs, *Sol. Energy Mater. Sol. Cells*, 2009, **93**, 465–475.
16 C. Girotto, D. Moia, B. P. Rand and P. Heremans, *Adv. Funct. Mater.*, 2011, **21**, 64–72.
17 A. Colsmann, M. Reinhard, T. H. Kwon, C. Kayser, F. Nickel, J. Czolk, U. Lemmer, N. Clark, J. Jasieniak, A. B. Holmes and D. Jones, *Sol. Energy Mater. Sol. Cells*, 2012, **98**, 118–123.
18 T. Wang, N. W. Scarratt, H. A. Yi, A. D. F. Dunbar, A. J. Pearson, D. C. Watters, T. S. Glen, A. C. Brook, J. Kingsley, A. R. Buckley, M. W. A. Skoda, A. M. Donald, R. A. L. Jones, A. Iraqi and D. G. Lidzey, *Adv. Energy Mater.*, 2013, **3**, 505–512.
19 S. F. Tedde, J. Kern, T. Sterzl, J. Furst, P. Lugli and O. Hayden, *Nano Lett.*, 2009, **9**, 980–983.

20 G. E. Eperon, V. M. Burlakov, P. Docampo, A. Goriely and H. J. Snaith, *Adv. Funct. Mater.*, 2014, **24**, 151–157.
21 P. Docampo, J. M. Ball, M. Darwich, G. E. Eperon and H. J. Snaith, *Nat. Commun.*, 2013, **4**, 2761.
22 J. You, Z. Hong, Y. M. Yang, Q. Chen, M. Cai, T. B. Song, C. C. Chen, S. Lu, Y. Liu, H. Zhou and Y. Yang, *ACS Nano*, 2014, **8**, 1674–1680.
23 G. E. Eperon, V. M. Burlakov, A. Goriely and H. J. Snaith, *ACS Nano*, 2014, **8**, 591–598.
24 A. Dualeh, N. Tétreault, T. Moehl, P. Gao, M. K. Nazeeruddin and M. Grätzel, *Adv. Funct. Mater.*, 2014, **24**, 3250–3258.
25 B. Conings, L. Baeten, C. De Dobbelaere, J. D'Haen, J. Manca and H. G. Boyen, *Adv. Mater.*, 2014, **26**, 2041–2046.
26 H. S. Kim, C. R. Lee, J. H. Im, K. B. Lee, T. Moehl, A. Marchioro, S. J. Moon, R. Humphry-Baker, J. H. Yum, J. E. Moser, M. Gratzel and N. G. Park, *Sci. Rep.*, 2012, **2**, 591.
27 W. Abu Laban and L. Etgar, *Energ Environ. Sci.*, 2013, **6**, 3249–3253.
28 B. Cai, Y. D. Xing, Z. Yang, W. H. Zhang and J. S. Qiu, *Energ Environ. Sci.*, 2013, **6**, 1480–1485.
29 Z. Xiao, C. Bi, Y. Shao, Q. Dong, Q. Wang, Y. Yuan, C. Wang, Y. Gao and J. Huang, *Energ Environ. Sci.*, 2014, DOI: 10.1039/c4ee01138d.
30 Q. Chen, H. Zhou, Z. Hong, S. Luo, H. S. Duan, H. H. Wang, Y. Liu, G. Li and Y. Yang, *J. Am. Chem. Soc.*, 2014, **136**, 622–625.
31 J. Griffin, A. J. Pearson, N. W. Scarratt, T. Wang, D. G. Lidzey and A. R. Buckley, *Org. Electron.*, 2014, **15**, 692–700.
32 L. M. Chen, Z. Hong, W. L. Kwan, C. H. Lu, Y. F. Lai, B. Lei, C. P. Liu and Y. Yang, *ACS Nano*, 2010, **4**, 4744–4752.
33 C. Girotto, B. P. Rand, J. Genoe and P. Heremans, *Sol. Energy Mater. Sol. Cells*, 2009, **93**, 454–458.
34 H. J. Snaith, A. Abate, J. M. Ball, G. E. Eperon, T. Leijtens, N. K. Noel, S. D. Stranks, J. T. W. Wang, K. Wojciechowski and W. Zhang, *J. Phys. Chem. Lett.*, 2014, **5**, 1511–1515.
35 M. Saliba, K. W. Tan, H. Sai, D. T. Moore, T. Scott, W. Zhang, L. A. Estroff, U. Wiesner and H. J. Snaith, *J. Phys. Chem. C*, 2014, DOI: 10.1021/jp500717w.

